Journal of Catalysis **197,** 98–112 (2001)
doi:10.1006/jcat.2000.3064, available online at http://www.idealibrary.com on IDEAL®

The Origin of the C_7-Hydroconversion Selectivities on Y, β, ZSM-22, ZSM-23, and EU-1 Zeolites

Pascal Raybaud,* Anne Patrigeon,† and Hervé Toulhoat*

*Division Informatique Scientifique et Mathématiques Appliquées, Institut Français du Pétrole, 1 and 4 avenue de Bois-Preau, 92852 Rueil-Malmaison Cedex, France; and †Division Cinétique et Catalyse, Institut Français du Pétrole, 92852 Rueil-Malmaison Cedex, France

Received May 22, 2000; revised September 18, 2000; accepted September 18, 2000

We carry out experimental hydroconversion tests of *n*-heptane paraffin on five different zeolites: Y, β, ZSM-22, ZSM-23, and EU-1. The experimental selectivities clearly depend on the catalyst pore structures. Through force field simulations, we investigate adsorption and diffusion properties as well as model cyclopropane intermediate stabilities inside each zeolite framework. In open structures such as Y and β, no shape transition state selectivity or diffusion limitation are taking place. In the more restricted 10-membered ring (MR) channels of ZSM-22, ZSM-23, and 10-MR windows of EU-1, we show that the selectivities in branched isomers and cracked products are explained by the combined effects of transition state restriction and product diffusion limitations. In particular, the selectivities in monomethyl-branched products are correlated to their relative diffusion barriers, in agreement with earlier results of E. B. Webb III *et al.* (1999, *J. Phys. Chem. B* 103, 4949). The explanation for this result has its foundation in the degree of symmetry of the monomethyl-branched paraffin. In ZSM-22 and ZSM-23, the 2,2- and 3,3-dMC$_5$ are not formed on account of transition-state shape restrictions, whereas a slight amount of 2,3- and 2,4-dMC$_5$ is formed and can diffuse out of the pores. In the EU-1 sieve, the large side pockets behave as the open Y or β structures, where all isomerization reactions can take place without restriction, but only the faster diffusing 2,3-dMC$_5$ and 2,4-dMC$_5$ products are released. The slower diffusing multibranched 2,2-dMC$_5$ and 3,3-dMC$_5$ paraffins are transformed via methyl shift or cracked inside the pockets producing a higher amount of cracked products in EU-1 than in ZSM-22 or ZSM-23.

Key Words: **paraffin hydroconversion; hydroisomerization; zeolites; molecular simulation; force field calculation; adsorption; diffusion properties; molecular shape selectivity.**

INTRODUCTION

According to new environmental specifications, the refining industry has to produce high-octane index fuels with lower aromatic contents. Indeed, the existing refining units such as reforming or catalytic cracking produce fuels with high aromatic contents. Processes avoiding aromatic products are already industrially used to boost the octane level: aliphatic alkylation, branched-ether synthesis, and hydroconversion of linear C_5 and C_6 hydrocarbons (1). In the latter, the light gas octane number is improved by increasing the degree of isoparaffin branching. For instance the 2,2-dimethyl-butane exhibits a Research Octane Number (RON) 91.8, whereas the *n*-hexane RON is only 24.8. Among C_7-paraffins, the trimethyl-butane RON is 112.1, while the *n*-heptane RON is zero. The dimethyl-pentane paraffins exhibit RONs between 80.8 and 92.8. Nevertheless, no industrial hydroisomerization process exists for the C_7 or C_8 paraffins because of their higher tendency to be cracked. The challenge for the research in that area is to find a catalyst favoring the isomerization of *n*-heptane and *n*-octane into high octane number multibranched isomers without too much cracking. One of the goals of the present work is to better understand how the experimental selectivity of C_7-hydroconversion is controlled in five different molecular sieve-supported platinum catalysts.

It is generally accepted that for a Pt-promoted zeolite catalyst, hydroisomerization occurs via the so-called bifunctional mechanism involving (de)hydrogenation steps on the metallic site and carbenium formations with rearrangement on the acidic site (2–5). On the metallic sites, the paraffin is dehydrogenated and the olefinic intermediates are formed (3, 6, 7). Further, the intermediates are either isomerized or cracked on the acidic sites. Two kinds of isomerization are distinguished. The type-A isomerization occurs via methyl or ethyl shift and simultaneous hydride shift (8, 9): the degree of branching is not modified. For the type-B isomerization, the chain length is modified and the intermediates are protonated cyclopropanes (PCP) (10, 11). At the same time, the hydrocarbon chain cracking considered as a competitive and unwished secondary reaction of C_7-hydroisomerization can take place through carbocation β-scission.

If the experimental conditions ensure that the hydrogenation function and the acid function are well balanced (12), the (de)hydrogenation reaction is not the rate-determining step, and the selectivity depends on the acidic properties or on the solid porosity. Three main proposals have been put forward to explain the selectivity in zeolite framework (13, 14).

0021-9517/01 $35.00

First the selectivity might be governed by the reactants themselves which are too bulky to enter the zeolite porosity and hence are not transformed.

Then, the selectivity can be governed by the products. On account of sterical hindrance, some products cannot diffuse out of the zeolite framework. It occurs in the toluene alkylation on ZSM-5, yielding a mixture of xylenes. The faster diffusing *para*-xylene is the major product recovered. For the isomerization reactions, it has been recently proposed by Webb III *et al.* (15, 16) on account of a molecular simulation study, that the selectivity of monomethyl-branched paraffins in molecular sieves follows their diffusion coefficients in various restricted molecular sieves.

Finally the selectivity may be governed by the shape or the bulkiness of the transition state intermediates such as protonated cyclopropanes (PCP) formed during the isomerization. This proposal has been put forward by Ernst *et al.* (17) to explain the selective *n*-decane isomerization in ZSM-22. More recently Mériaudeau *et al.* (18) also retain this concept for the selective hydroisomerization of C_8 in SAPO molecular sieves. Maesen *et al.* (19) proposed to combine diffusion selectivity with PCP selectivity to understand the isomerization of paraffins in TON, MTT, and AEL zeolites. Nevertheless, no clear evidence coming from experimentation or simulation on dimethyl-branched isomers has been proposed for the time being to support the latter proposal.

At this stage, the following preliminary remarks on the transition state selectivity concept should be made. The (de)stabilization of the PCP intermediate depends on two different kinds of interactions within the zeolite pores. On the one hand, the local chemical interactions of the protonated cyclopropanic ring with the acidic sites influence the energy barriers of the hydroisomerization steps. On the other hand, the zeolite framework via long-range interactions contributes to the relative stability of PCPs according to their bulkinesses: this is generally referenced (and will be so in this paper) to the "shape transition state selectivity." The latter contribution plays a role all the more crucial as the zeolite structure exhibits channel diameters close to the PCP sizes as it will be shown in this paper.

Another concept called "pore mouth" and "key-lock" has been proposed by Martens *et al.* (20–23) to explain the paraffin hydroisomerization selectivity observed in ZSM-22. Due to sterical hindrance the monomethyl-branched C_7-isomers adsorption inside the pores would be prevented (20). The isomerization reaction would take place on the pore mouth of the ZSM-22 channels. The stronger the adsorption constant on the pore mouth of one given isomer, the higher the amount of this isomer would be formed. This scheme requires to take into account entropic effects as the main factors able to differentiate the adsorption constants through the preexponential factors. Nevertheless, the pore mouth formalism first proposed in (20) and claiming that the adsorption of monobranched isomers cannot occur inside the ZSM-22 pores using molecular graphic consideration does not find a general agreement within the scientific community (19). From the analysis of the elementary steps of the reaction mechanism, it is legitimate to wonder why the 2-monomethyl-branched products observed in majority should exhibit the highest adsorption energy at the pore mouth. Once the monobranched isomer is formed, it can undergo two competitive reaction pathways: either it desorbs as a final product or it further reacts by isomerization or cracking. It sounds contradictory to claim that the most strongly adsorbed isomer will be the one that desorbs preferentially. Actually "moderate" adsorption energies would offer the best compromise: a not too weak energy stabilizes the formation of the isomer while a not too strong one prevents it from remaining stuck at the pore mouth. Therefore the pore mouth concept cannot be considered as fully established, and further investigation is needed to nurture the debate.

In order to investigate some of the proposals put forward above, we have carried out *n*-heptane hydroconversion tests with five different molecular sieves: Y, β, ZSM-22, ZSM-23, and EU-1. As has been recently shown in a previous study (24), these catalytic systems exhibit rather different porosities that lead to different selectivities among mono-branched, dimethyl-branched, and cracked products. Simultaneously we have simulated adsorption and diffusion properties through force field molecular modeling for all the C_7-isomers. A first attempt to simulate the long-range interaction of the zeolite framework with model transition states involving a three-membered ring cyclopropane (CP) molecule is also made.

The first part of the paper presents the experimental conditions for the preparation of the catalytic systems and for the C_7-hydroconversion tests. In this part, we also present the methodology used for the adsorption and diffusion simulations. In the second part, the experimental and simulation results are described in detail. Finally we discuss these results and furnish an explanation of the selectivities observed on the five molecular sieves.

METHODS

A. Experiments

The hydroconversion of *n*-heptane is studied on Y, β, EU-1, ZSM-22, and ZSM-23 zeolites. The structure type code, the dimensionality, the size of oxygen member rings and the cross-sectional dimensions of channels are given in Table 1. The ZSM-22 and ZSM-23 zeolites have one-dimensional uninterrupted channel structures. They differ only by the dimensions of the channels. The zeolite EU-1 also has a one-dimensional 10-MR channel system, but periodically interrupted by alternating "side pockets."

TABLE 1

Main Characteristics of the Catalytic Systems

Structure (Ref.)	Code	D[a]	Windows[b]	Channel dimensions (Å)	$(Si/Al)_G$	S_{BET} (m^2/g)
Y (25)	FAU	3	12 MR	7.4	16	824
β (26)	BEA	3	12 MR	$7.6 \times 6.4 + 5.5 \times 5.5$	13	678
ZSM-22 (27)	TON	1	10 MR	4.4×5.5	36	157
ZSM-23 (28)	MTT	1	10 MR	4.5×5.2	20	252
EU-1 (29)	EUO	1	10 MR	4.1×5.7 + large side pockets	16	402

[a] Dimensionality of the porous structure.
[b] MR, member ring of oxygen atoms.

That is why this can be regarded more precisely as 10-MR "windows." In this structure, the mouths of the pockets are formed by 12-MRs with a cross section of 6.8×5.8 Å and each side pocket is 8 Å deep (30). The Y and β zeolites have three-dimensional 12-MR channel structures. In the Y zeolite, large supercages (12.3 Å of diameter) are formed by the channel intersections.

1. *Preparation and Characterisation of Catalysts*

The Y- and β-zeolites are commercial zeolites from Tosoh and Zeolyst, respectively. The EU-1 zeolite was synthesized according to procedure described in (31). The ZSM-22 and ZSM-23 zeolites were synthesized according to (32) and (33), respectively, and were calcined at 550°C under oxygen flow to remove any residual organic compound. The NH_4 form of the zeolites was obtained by slurrying them three times in a 10 M ammonium nitrate solution (10 mL per gram of solid) at 100°C. The NH_4 zeolite sample were loaded with 1 wt% Pt by incipient wetness impregnation using $Pt(NH_3)_4Cl_2$ as precursor. The solids were then calcined under air flow at 420°C for 4 h to decompose the platinic salt and obtain the H zeolite form. The main characteristics of the solids are presented in Table 1. The global silicon to aluminum atomic ratios $(Si/Al)_G$ were determined by X-ray fluorescence and the specific surface areas (S_{BET}) by nitrogen adsorption isotherm recorded at 77 K according to the BET method. The high crystallinity of the molecular sieves was verified by X-ray diffraction.

2. *Catalytic Tests*

The *n*-heptane conversion was carried out at atmospheric pressure under a hydrogen flow in a fixed-bed microreactor. The reduction stage was performed at 450°C in a hydrogen flow of 5 L/h/g of catalyst. Then the temperature was then decreased and fixed to a value depending on the catalyst activity (Table 2). The *n*-heptane conversion was changed by varying the contact time (defined as the inverse weight liquid hourly space velocity, WLHSV). The molar ratio $H_2/n\text{-}C_7$ was chosen equal to 2. The reaction products were analyzed on-line using a GC with a FID detector and a HP-PONA (50 m × 0.2 mm) capillary column.

As the solids studied have different concentrations of acidic sites, we have tested the influence of the $(Si/Al)_G$ ratio. Three β-zeolites with $(Si/Al)_G$ equal to 13, 30, and 94 have been tested, the two latter being obtained by nitric acid treatment of the first one. As these solids exhibited different activities, they were tested at different temperatures (210, 230, and 260 respectively) and at a same pressure (1 bar), but revealed identical selectivities in *n*-heptane conversion.

B. Molecular Simulation

For the simulation, we have used two main approaches: on the one hand, we have calculated adsorption enthalpies at low coverages for the different C_7-isomers and for the cyclopropanic model intermediates. On the other hand, we have established detailed energy profiles of relevant isomers along the diffusion path inside the ZSM-22, ZSM-23 channels and across the EU-1 windows. The simulation engines are Sorption and Diffusion-Path accessible through the Cerius^2 (release 4.0) and InsightII (release 4.0.0P+) interfaces licensed by Molecular Simulation Inc. (34). The Sorption module is used for calculating the adsorption enthalpies thanks to a Monte Carlo technique and the Diffusion-Path module for determining the energy profiles along the diffusion path (35).

1. *Force Field*

We treat the molecule–zeolite interaction at an atomic level assuming that we can neglect the precise electron distribution for focusing on the main environmental effect

TABLE 2

Hydroconversion Test Conditions for the Solids Studied

Structure	T (°C)	P (bar)	t (h)	$H_2/n\text{-}C_7$
Y	250	1	0.1–2	2
β	210	1	0.2–2	2
ZSM–22	240	1	0.1–6	2
ZSM–23	230	1	0.2–2	2
EU–1	220	1	0.3–2	2

due to the different porous properties. So we ignore the electron–ion and electron–electron interaction. This would be required for the investigation of real transition states. For that purpose, we have used the Condensed-Phase Optimized Molecular Potentials for Atomistic Simulation Studies (Compass) force field (36). The potential energy, E_{total}, of a molecule in the pores depends on its atomic coordinates and can be expressed as the sum of valence-bond terms and nonbond interaction terms. The parameters for the valence terms are fitted on *ab-initio* calculated data using least-square-fitting techniques (37) and corrected by empirical adjustments on molecular structures, molecular dipole moments, vibrational frequencies, and conformational energies.

The nonbond interaction term stands for the long interactions between the paraffin atoms themselves and between the paraffin atoms and the zeolite framework. The nonbond interactions are the sum of two contributions: the van der Waals interaction and the electrostatic (or coulombic interaction). The van der Waals forces are described by a Lennard-Jones 9–6 interaction. The nonbond parameters are determined empirically by fitting simulated thermophysical properties with experimental data. The Compass force field contains LJ parameters for like atom pairs. The nondiagonal terms are evaluated through a sixth-order combination law. The electrostatic interactions are represented using atomic partial charges.

For the simulation of alkane adsorptions the zeolite framework is represented by a repeated unit cell with three-dimensional periodic boundary conditions. The van der Waals interactions are considered only in a sphere within a finite radius, called the cutoff radius using the with long-range tail correction (38). In order not to generate a periodicity for the adsorbate, the cutoff radius has to be inferior to half of the smallest cell parameter. Nevertheless, the cutoff value should be converged with respect to the energy. We have found that a cutoff radius of 20 Å allows the best compromise between the accuracy and the calculation time required for all the systems described by a supercell for which all cell parameters are greater than 40 Å.

Adsorption enthalpy calculation. We have used the Monte Carlo technique to investigate the adsorption configuration of the paraffins inside the pores, and estimate the adsorption enthalpies for a given temperature ($T = 503$ K) at low coverages (close to the Henry regime). At low temperature the location and binding energy of a sorbate molecule may be readily determined by energy minimization. However, at ambient temperatures, paraffins within the zeolite framework are distributed over several sites; the "location" becomes a probability distribution and energy an integral over all accessible sites. We have chosen to keep fixed the paraffin loading equal to 1 molecule per cell so that the corresponding coverage for the size of the cell remains close to the Henry regime. For the canonical ensemble (NVT), the Metropolis algorithm proceeds by selecting, and displacing randomly, a molecule. The energy of the new trial state is calculated and the state is accepted if:

$$E_{\text{trial}} < E_{\text{initial}} \qquad [1]$$

or if

$$\exp\{-(E_{\text{trial}} - E_{\text{initial}})/kT\} < \text{rand}(0, 1), \qquad [2]$$

where E_{initial} and E_{trial} are the total energies of the system before and after the molecule displacement, respectively, T is the temperature and k the Boltzmann's constant.

The Metropolis scheme generates Markov chain of states which sample the equilibrium states of the system according to the Boltzmann probability distribution. Depending on the system and on the paraffins, the number of search iterations varies between 10^6 and 5×10^6 before reaching the convergence criterion on the energy (0.1 kJ/mol).

The atoms of the zeolite framework are kept fixed and the paraffins are supposed not to be flexible.

Adsorption enthalpies for intermediate compounds. The complete and exact determination of the stability of the well-known hypothetical protonated cyclopropane (PCP) transition states on the acidic sites is far beyond the scope of this study. A precise investigation of the nature of the active site would be a prerequisite, on the one hand. The study of the PCPs stabilities on the active sites would require *ab initio* techniques like the density functional theory (DFT), on the other hand. In the present work, we propose to investigate the stability of the cyclopropane (CP) compound corresponding to the PCP intermediates as depicted on Fig. 6a. In such a way, we study whether the long-range interactions with the zeolite framework play a role on the selectivity through sterical hindrances in restricted zeolite structure such as ZSM-22, ZSM-23, and EU-1.

We calculate adsorption enthalpies at low coverages for the CP derived from each PCP intermediate. This will be described in more details in the next Part. We use the Monte Carlo procedure in the (NVT) ensemble (already described in the previous paragraph) for finding the most favorable CP adsorption configurations. In order to take into account the geometry relaxation of the CP that is more critical than for reactants, the CP configurations are chosen among a sample obtained by a 100-ps molecular dynamic simulation ($T = 503$ K) for the isolated CP.

2. *Diffusion Path Simulations*

We determine the energy profiles along the diffusion path of relevant C_7-isomers and compare the energy barriers for paraffins with the same degree of branching inside ZSM-22, ZSM-23, and EU-1 zeolites. The energy profiles are also calculated for monomethyl-branched isomers with longer chains such as C_{10} and C_{16} inside the ZSM-22.

The diffusion path calculation is carried out on zeolite clusters as shown schematically on Fig. 1. The channel length used for the simulation varies between 30 and 50 Å

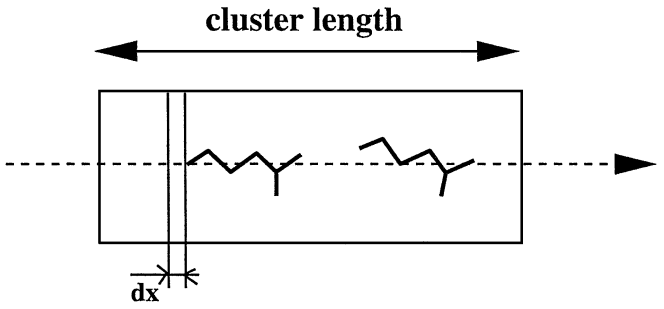

FIG. 1. Schematic representation of the zeolite clusters used for the diffusion path simulation. dx stands for the motion step equal to 0.1 Å.

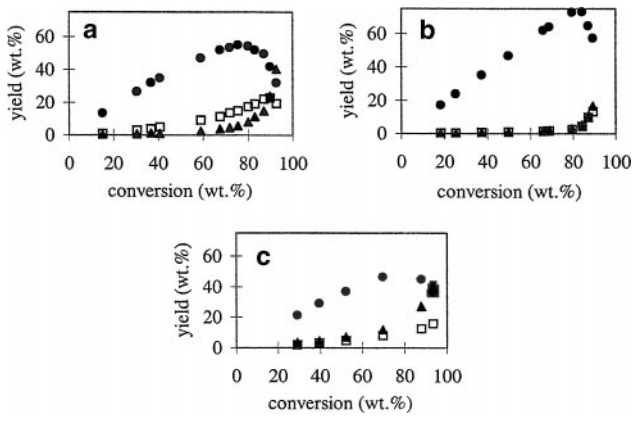

FIG. 2. Yield in monobranched isomers (●), yield in multibranched isomers (□); and yield in cracked products (▲) obtained on (a) Pt/H-Y at 250°C or Pt/H-β zeolites at 210°C, (b) Pt/ZSM-22 and Pt/ZSM-23 at 240°C, and (c) Pt/EU-1 at 220°C.

according to the systems, this size is sufficient enough to study relevant diffusion paths. For the sake of clarity, the energy profiles will be plotted for a channel length of 15 Å only. The initial pathway is assumed to be a straight line following the channel symmetry axis and connecting two positions located at the center of the pore at a distance of a cluster length. Then the paraffin is forced to move along this pathway by steps of d$x = 0.1$ Å. At each step, the geometry of the paraffin is optimized, allowing atomic displacements in a plane perpendicular to the initial pathway, while the zeolite cluster is kept rigid. This calculation provides an energy profile along the diffusion pathway. This profile can be used to estimate diffusion barriers, under the approximation that entropic contributions to the free energy profile are negligeable.

RESULTS

A. Experiments

Under the experimental conditions, the Y- and β-zeolites lead to very similar yields as reported on Fig. 2a and Table 3. At low conversion, the monobranched isomers are predominant: they are clearly primary products of the reaction. When the nC$_7$ conversion increases, the yield in monobranched products reaches a maximum (54 wt%) and then decreases. The yield in multibranched, which is very low at low conversion, also increases with the conversion, goes through a maximum (25 wt%) and then decreases. The maximum yield in multibranched products is shifted toward the higher conversions compared to the maximum yield in monobranched products, which shows that the formation of multibranched products is consecutive to the formation of monobranched isomers. The cracked products appear at medium conversion (60 wt%) and increase strongly at high conversion. They are clearly secondary products of the reaction. According to these results, the overall reaction scheme can be written

$$n\mathrm{C}_7 \rightleftarrows \mathrm{MB} \rightleftarrows \mathrm{MuB} \rightarrow i\mathrm{C}_4 + \mathrm{C}_3, \qquad [3]$$

TABLE 3

Molar Fractions of the Different Produced Paraffins for a C$_7$-Conversion of about 30 and 80%

Catalyst:	Y		ZSM-22		ZSM-23		EU-1	
Conversion (%wt):	26.0	83.1	24.8	78.7	31.9	78.1	29.2	79.7
Contact time (h):	0.111	0.833	0.143	1.000	0.250	1.000	0.333	1.000
n-C$_7$	0.740	0.169	0.749	0.207	0.675	0.211	0.708	0.203
2-MC$_6$	0.103	0.226	0.157	0.381	0.185	0.370	0.111	0.209
3-MC$_6$	0.105	0.227	0.079	0.316	0.112	0.305	0.091	0.203
3-EtC$_5$	0.007	0.017	0.001	0.006	0.001	0.006	0.003	0.010
2,2-dMC$_5$	0.005	0.049	0.000	0.001	0.000	0.001	0.001	0.009
2,4-dMC$_5$	0.011	0.059	0.003	0.024	0.005	0.022	0.011	0.039
3,3-dMC$_5$	0.002	0.026	0.000	0.000	0.000	0.000	0.000	0.003
2,3-dMC$_5$	0.015	0.067	0.001	0.004	0.002	0.010	0.008	0.031
2,2,3-tMC$_4$	0.000	0.007	0.000	0.000	0.000	0.000	0.000	0.000
C$_3$	0.004	0.068	0.004	0.026	0.008	0.032	0.030	0.133
i-C$_4$	0.004	0.069	0.002	0.012	0.006	0.022	0.029	0.133
n-C$_4$	0.000	0.004	0.002	0.013	0.002	0.009	0.002	0.007

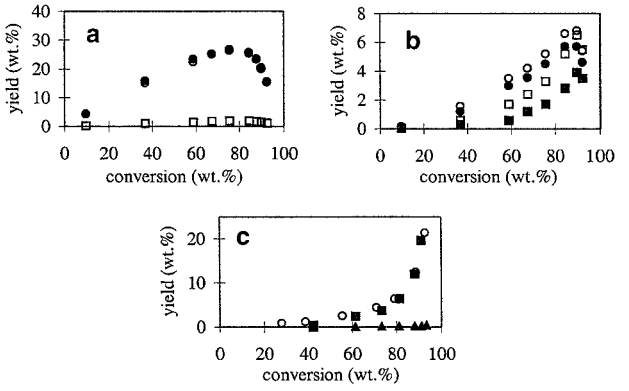

FIG. 3. Catalytic results on Pt/H-Y or Pt/H-β. (a) Yields in monobranched isomers (●) 2-MC_6, (○) 3-MC_6, (□) 3-EC_5; (b) yields in multibranched isomers (●) 2,4-dMC_5, (○) 2,3-dMC_5, (■) 3,3-dMC_5, (□) 2,2-dMC_5; (c) yields in cracked products (○) propane, (■) iso-butane, (▲) *n*-butane.

where MB stands for the monobranched products and MuB for the multibranched products.

The 2-MC_6 and the 3-MC_6 are formed in same quantities whatever the nC_7 conversion (see Fig. 3a and Table 3) as predicted by the thermodynamic equilibrium. Among the multibranched isomers, four dM-C_5 are formed and the 2,4-dMC_5 and 2,3-dMC_5 are predominant until 80 wt% of conversion as shown on Fig. 3b. As for the cracked products, iso-butane and propane are approximately formed in same quantities, attesting that 2,2-dMC_5 and 2,4-dMC_5 are the isomers which crack predominantly (9).

The selectivities from *n*-heptane conversion obtained on Pt/ZSM-22 and Pt/ZSM-23 are strongly different from those of Pt/H-Y or Pt/H-β. In ZSM-22 almost all the isomers formed are monobranched even at high conversions. A monobranched yield of 73 wt% is observed at 84 wt% *n*-heptane conversion (Fig. 2b). Cracking is very low: 6 wt% at 84 wt% conversion. Until 85 wt% of conversion, 2-MC_6 is obtained in higher amount than the 3-MC_6 (Fig. 4a and Table 3). Until very high conversions, no dimethylpentane with geminal methyl groups are formed and 2,4-dMC_5 is obtained preferentially compared to 2,3-dMC_5 (Fig. 4b). Among the cracked products, a significant amount of *n*-butane is formed (Fig. 4c) in contrast with Y- or β-zeolite, which proves that the cracking mechanism is different on Pt/ZSM-22.

On Pt/ZSM-23, slight differences with ZSM-22 are detected in selectivities as reported in Table 3. Among the monobranched isomers, 2-MC_6 is less favored than 3-MC_6 on ZSM-22. For multibranched isomers, the yield in 2,3-dMC_5 is slightly higher than on ZSM-22. The amount of cracked products is also slightly higher in ZSM-23 for conversions reported in Table 3, the smaller amount of nC_4 is balanced by higher quantities of C_3 and iC_4.

On Pt/EU-1, the cracking selectivity is higher than on Pt/H-Y or Pt/H-β (see Fig. 2c). The monobranched isomers are predominant at low and medium conversions. However, in contrast to H-Y or H-β, beyond 50 wt% conversion, the cracking yield is higher than the multibranched yield. At low conversion, 2-MC_6 is slightly predominant compared to the 3-MC_6 (Fig. 5a). Among the dibranched isomers which are all formed, dimethylpentanes with geminal methyl groups are disfavored (Fig. 5b). As for the cracked products, iso-butane and propane are approximately formed in same quantities like on H-Y and H-β (Fig. 5c). As may be predicted on the basis of its intermediate pore size, the selectivities obtained on Pt/EU-1 are somewhere in between those obtained for the Y- or β-zeolites and for ZSM-22.

As a first conclusion on the catalytic results, it appears that the solid porosity has a strong influence on the products of the *n*-heptane conversion. Selectivities of isomerization and cracking as well as selectivities among monobranched

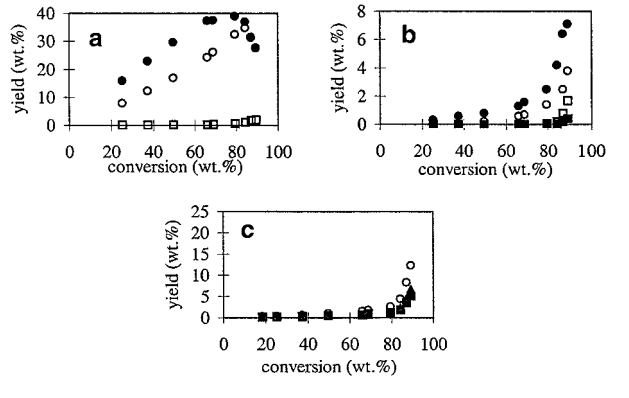

FIG. 4. Catalytic results on Pt/ZSM-22. (a) Yields in monobranched isomers (●) 2-MC_6, (○) 3-MC_6, (□) 3-EC_5; (b) yields in multibranched isomers (●) 2,4-dMC_5, (○) 2,3-dMC_5, (■) 3,3-dMC_5, (□) 2,2-dMC_5; (c) yields in cracked products (○) propane, (■) iso-butane, (▲) *n*-butane.

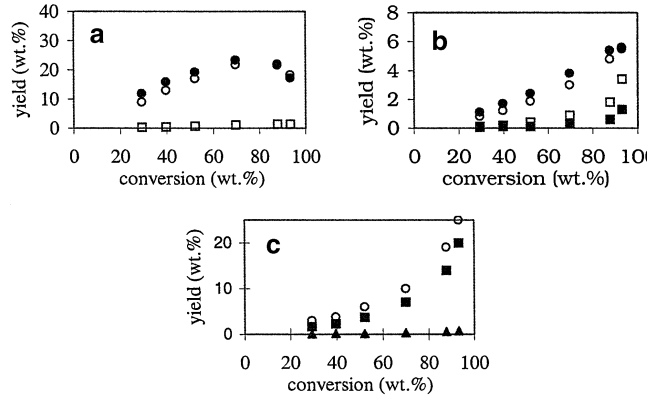

FIG. 5. Catalytic results on Pt/EU-1. (a) Yields in monobranched isomers (●) 2-MC_6, (○) 3-MC_6, (□) 3-EC_5; (b) yields in multibranched isomers (●) 2,4-dMC_5, (○) 2,3-dMC_5, (■) 3,3-dMC_5, (□) 2,2-dMC_5; (c) yields in cracked products (○) propane, (■) iso-butane, (▲) *n*-butane.

isomers or among multibranched isomers are quite different depending on the zeolite structure as it has already been mentioned in other experimental studies (19, 24).

B. Simulation

1. *Product Adsorption Enthalpies at Low Coverage*

Table 4 reports the adsorption enthalpies at low coverage we have calculated for the five zeolite systems using the Compass force field. The comparison with the experiments of Denayer *et al.* (39) is made for four zeolites, Y, β, ZSM-23, and ZSM-22. We also add the recent results by Maesen *et al.* (19) using similar simulation procedures (GCMC) but a different force field (40).

We observe first that the agreement between the calculated and experimental adsorption enthalpies is quite good for the four porous systems for which we have experimental data. We have added the reference case of silicalite although no hydroisomerization test have been carried out on it. The results are consistent with those for the other structures and provide reference data for comparison of the Compass FF to other approach. The Compass force field is rather robust, which is not surprising since it contains *ab initio* fitted parameters for the bonding interactions on the one hand and since some of the nonbonding interaction parameters are fitted to zeolite systems on the other hand. It also includes nondiagonal terms. The force field developed by Vlugt *et al.* (40) seems to improve even more the energetic values on restricted structures such as ZSM-22. The explanation might come from the fact that this force field is fitted on silicalite, the silica analog of ZSM-5, which exhibits similar porous properties to ZSM-22.

If we consider the relative enthalpy values obtained for the five different systems, we can notice they are also in nice agreement with the experimental data (see Table 4). For the open structures with 12-MR channels, such as Y- and β-zeolites, there is only small variations of the adsorption enthalpy values versus the different isomers (between −45.8 kJ/mol and −50.0 kJ/mol). This is also observed experimentally. Even for multibranched paraffins the repulsive interactions are rather weak so that the molecules can always find rooms in the 12-MR pore to optimize their adsorption configuration.

For the restricted ZSM-23 and ZSM-22 structures, the calculated (or experimental) adsorption enthalpies vary significantly versus the kind of C_7-isomer: between −31.6 and −104 kJ/mol for ZSM-22 and between −39.8 and −97.8 kJ/mol for ZSM-23, respectively. For both systems, the Monte-Carlo sampling did not find any 2,2,3-tMC_4 adsorbed in ZSM-22 or ZSM-23 and 2,2dMC_5 in ZSM-22 even after 5 million tries. The higher the degree of branching, the lower the adsorption enthalpy. This might be a strong argument in favor of product adsorption selectivity in restricted structures. This result reveals also that 2,2-dMC_5, 3,3-dMC_5, and 2,2,3-tMC_4 do not fit in ZSM-22. We also notice that the adsorption enthalpies of 2-MC_6 are higher than that of the 3-MC_6 inside the pores of these structures. Nevertheless, the adsorption enthalpies calculated for different dimethyl-branched C_5 isomers in ZSM-22 or ZSM-23 cannot be correlated to the experimental selectivies reported on Table 3. In ZSM-23, the 2,2- and 3,3-dMC_5 are adsorbed more strongly than 2,4- and 2,3-dMC_5, whereas they are not detected experimentally.

It is impossible to explain the results obtained on more complex porous media such as EU-1 where two different kinds of voids are present (10-MR windows and 12-MR side pockets). EU-1 exhibits adsorption enthalpies with no real distinctions among the different isomers as it was also the case for the Y- and β-zeolite. Nevertheless, this catalyst has experimental selectivities in multibranched products close to ZSM-23 or ZSM-22. Actually the large side pockets with 12-MR structures adsorb multibranched paraffins where

TABLE 4

Experimental (from Ref. 39), Calculated Adsorption Enthalpies (kJ/mol) of the Different C_7-Isomers at Low Coverage Inside Y, β, ZSM-22, ZSM-23, and EU-1 Zeolites

	FAU		BEA		MFI		ZSM-22			ZSM-23		EU-1
	Exp.	Our work	Exp.	Our work	Exp.	Our work	Exp.	Our work	Ref. 19	Our work	Ref. 19	Our work
n-C_7	−51.9	−50.0	−72.6	−74.9	−79.6	−95.2	−87.9	−104.0	−85.9	−97.8	−76.3	−92.4
2-MC_6	−51.6	−48.8	−70.4	−72.9	−78.4	−88.6	−75.4	−93.4	−84.6	−90.4	−69.7	−92.0
3-MC_6	−51.4	−48.9	−69.7	−73.1	−78.0	nc	−69.8	−84.7	−81.4	−74.7	−66.2	−91.1
3-EC_5	nr	−49.1	nr	−71.5	nr	nc	nr	−78.0	nr	−39.8	nr	−83.6
2,2-dMC_5	nr	−47.1	nr	−70.2	nr	nc	nr	—	nr	−68.1	nr	−88.9
2,4-dMC_5	nr	−47.4	nr	−71.5	nr	nc	nr	−70.3	nr	−62.8	nr	−92.7
3,3-dMC_5	nr	−47.3	nr	−71.4	nr	nc	nr	−31.6	+6.3	−71.5	−55.5	−84.4
2,3-dMC_5	−50.6	−48.4	−67.7	−70.7	−74.1	−81.9	−60.2	−78.3	−73.8	−50.6	−46.0	−90.0
2,2,3-tMC_4	nr	−45.8	nr	−67.7	nr	nc	nr	—	nr	—	nr	−84.2

Note. $T = 503$ K for our simulations (except for MFI at $T = 573$ K). The experimental data are at $T = 573$ K. Ref. 19 corresponds to the adsorption enthalpies calculated by Maesen *et al.* nr means no results found in the literature; nc means no values calculated within our work.

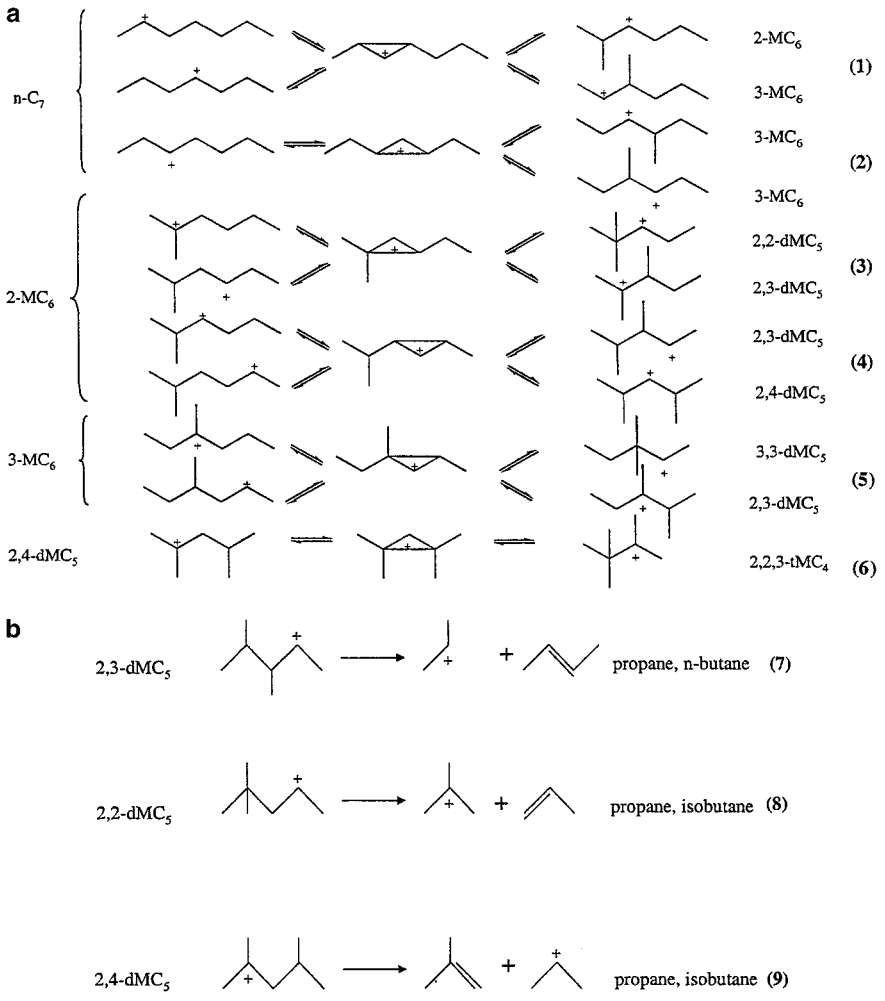

FIG. 6. (a) Isomerization mechanisms via protonated cyclopropane for *n*-heptane and isomers and (b) β-scission mechanisms of the *n*-heptane dibranched isomers.

the latter can find enough room with small repulsive interactions. In this case the product adsorption selectivity is rather weak, whereas the experimental selectivities are strong. From this point of view, the EU-1 behavior cannot be correlated to the adsorption enthalpies.

2. *Adsorption of CycloPropane (CP) Intermediates*

As it seems to be well established by several experimental studies reported in the literature (5, 9, 10), the isomerization reactions involve PCP intermediates. On Fig. 6, we represent the 1-methyl, 2-propyl PCP(1) and 2,2-ethyl PCP(2) intermediates involved in the isomerization of linear *n*-heptane into 2-MC_6 and 3-MC_6. For MC_6 isomerizations, three PCP intermediates are concerned: 1,1-dimethyl, 2-ethyl PCP(3) and 1-isopropyl, 2-methyl PCP(4) and 1,2-methyl, 2-ethyl PCP(5). As we have explained it in the previous part, we study only the relative stabilities of the corresponding CP(i) compounds inside the different porous media.

Table 5 reports the adsorption enthalpies for the five possible CP(i) intermediates. In ZSM-22, a strong environmental effect determines the relative CP stabilities. The adsorption enthalpies vary between −45 and −85 kJ/mol. The less stable CPs (3), (4), and (5) are those involved in the isomerization of methyl-branched isomers into dimethyl-branched

TABLE 5

Adsorption Enthalpies (kJ/mol) Calculated at Low Coverage and $T = 503$ K for the Five CycloPropanes (CP) Intermediates in ZSM-22, EU-1, and β-zeolites

Intermediates	ZSM-22	EU-1	β
1-Methyl, 2-propyl CP (1)	−85.6	−84.6	−68.2
2,2-Ethyl CP (2)	−82.4	−83.8	−67.6
1,1-Dimethyl, 2-ethyl CP (3)	−50.6	−83.6	−65.9
1-Isopropyl, 2-methyl CP (4)	−77.3	−83.1	−65.9
1,2-Methyl, 1-ethyl CP (5)	−45.8	−80.4	−63.7

Note. See also Fig. 6a for numbering.

products. Among those CPs, CP(4) is the most stable one. Within the approximations of our calculation, this appears as a relevant argument in favor of shape TS selectivity occurring in restricted structures.

In EU-1, as well as in the open β-zeolite, the stabilities of the different CP are the same no matter how the environmental effect may be. In EU-1, we observe again that the large side pockets offer enough rooms for all CPs to be formed without any selectivity influenced by the zeolite framework.

As a first conclusion we can already show that on restricted structures such as ZSM-22 or ZSM-23, the long-range interactions of the framework play a significant role on the (de)stabilization of intermediates. On open structures, this contribution is far less pronounced and the relative stabilities of the transition states would depend mainly on the local chemical interactions of the PCP rings with the acidic sites (see remarks in the Introduction).

B. Product Diffusion

1. *Monomethyl-Branched Products*

ZSM-22. First we present results obtained with the diffusion path method and compare them with molecular dynamic simulations on linear and monomethyl-branched zeolite recently proposed in the literature (15, 16). Figure 7a shows the energy profiles for *n*-heptane and monomethyl-branched C_6 isomers. The profiles exhibit clearly variations with a periodicity of 5 Å corresponding to the periodicity of the interactions with the sinusoidal zeolite channel. For the linear *n*-heptane, the energy profile is symmetric. The energy barrier is small and unambiguously identified as the difference between the global maximum and global minimum of the energy values. This yields +3.3 kJ/mol as reported in Table 6. For 2-MC_6 and 3-MC_6, the profiles are always periodical but not symmetric anymore so that we can identify three different energy barriers represented by the three arrows on Fig. 7. The difference between the global maximum and the global minimum yield +24.4 kJ/mol for 2-MC_6 (arrow 1). This barrier can be decomposed into two smaller barriers. The first one is the difference between the global maximum and the local minimum of the profile: +14.3 kJ/mol (arrow 2). The difference between the local maximum and the global minimum stands for the second barrier +10.8 kJ/mol (arrow 3). The actual barrier corresponds to the maximum of the two barriers, i.e., +14.3 kJ/mol. For 3-MC_6, we obtain a slightly higher value: +15.9 kJ/mol. This first result is in agreement with molecular dynamic simulation (15, 16), showing that 3-MC_6 diffuses slower than 2-MC_6.

We notice that the absolute values for this diffusion barrier remain quite reasonable, either for the linear or for the monomethyl-branched product. It could be easily overcome at $T = 503$ K (3 to 4 kT). The diffusion barrier of monomethyl-branched C_7-isomers are about 4.5 times higher than *n*-heptane.

For longer paraffin chains, the energy profiles plotted on Figs. 7b and 7c can be interpreted in a rather similar way

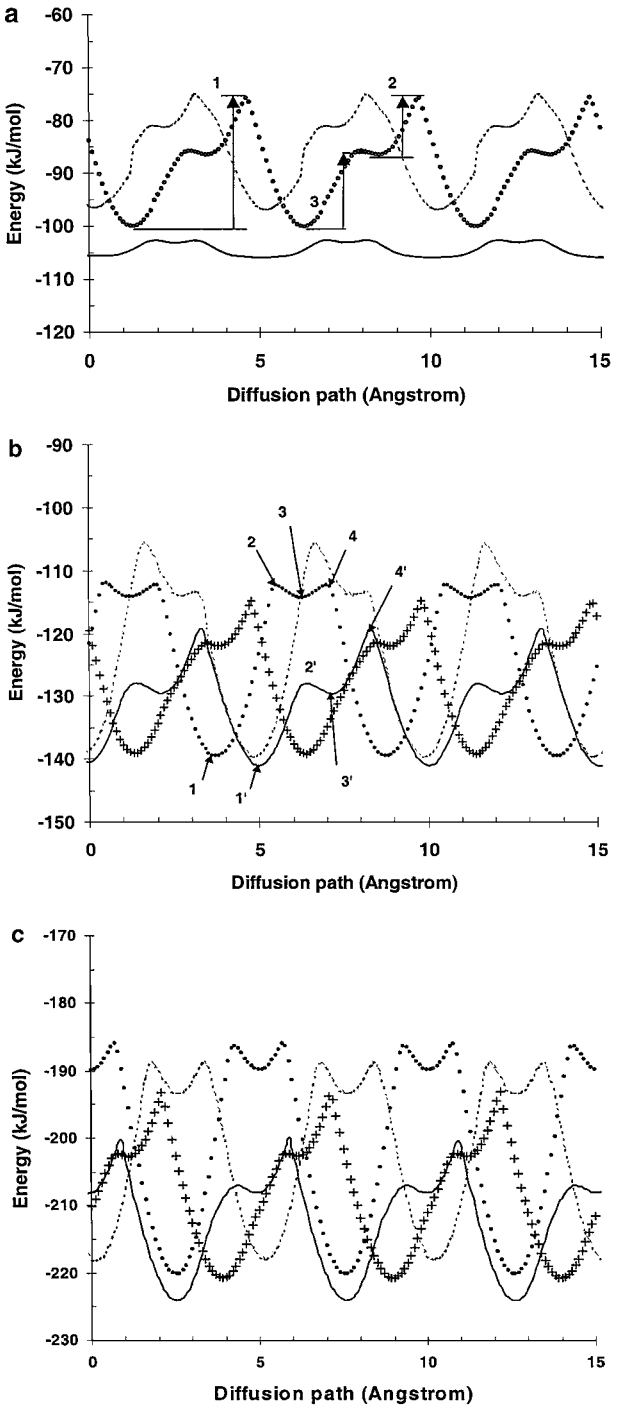

FIG. 7. Energy profiles along the diffusion path inside the ZSM-22 (001) channel of (a) nC_7 (—), 2-MC_6 (•••), and 3-MC_6 (- - -); (b) 2-MC_9 (—), 3-MC_9 (+++), 4-MC_9 (- - -), and 5-MC_9 (•••); (c) 2-MC_{15} (—), 3-MC_{15} (+++), 6-MC_{15} (•••), and 8-MC_{15} (- - -).

TABLE 6

Energy Optima (in kJ/mol) along the Diffusion Path of the Linear, Monomethyl-Branched, and 3-EC_5 Isomers in ZSM-22 and ZSM-23 Zeolites

	Energy minimum	Energy maximum	Energy barrier
ZSM-22			
n-C_7	−106.0	−102.7	+3.3
2-MC_6	−100.1	−75.7	+14.3
3-MC_6	−96.9	−75.2	+15.9
3-EC_5	−88.4	−43.6	+33.3
2-MC_9	−141.0	−119.3	+13.1
3-MC_9	−139.2	−114.5	+17.7
4-MC_9	−139.6	−105.8	+26.2
5-MC_9	−139.4	−112.3	+27.2
2-MC_{15}	−224.2	−200.4	+17.1
3-MC_{15}	−220.8	−193.8	+18.5
4-MC_{15}	−218.9	−188.2	+24.1
5-MC_{15}	−220.5	−186.5	+25.6
6-MC_{15}	−220.1	−186.4	+33.7
7-MC_{15}	−219.2	−186.3	+30.6
8-MC_{15}	−218.0	−188.9	+29.1
ZSM-23			
n-C_7	−99.2	−94.3	+4.9
2-MC_6	−93.6	−49.3	+44.3
3-MC_6	−86.6	−34.2	+52.5

Note. The geometry of the paraffins is optimized. We report the calculated energy barrier for the diffusion. The energy values correspond to the energy profiles represented on Figs. 7a, 7b, and 7c.

as proposed for C_7-isomers. 5-MC_9 and 8-MC_{15} exhibit a perfectly symmetric profile so that the energy barrier is unambiguously evaluated at +27.2 and +29.1 kJ/mol, respectively (see Table 6). In these two cases, the molecule is symmetric so that the lengths of the two chains on each side of the methyl group are the same, which implies the symmetric energy profiles. Figure 8a shows the four configurations corresponding to the global minimum (position 1), to the global maxima (positions 2 and 4) and to the local minimum (position 3) of 5-MC_9. Positions 2 and 4 are symmetric configurations. These correspond to two energy maxima with the same energy values because of the sterical hindrance of the two symmetric chains on each side of the methyl group.

For 2-MC_9 (as well as for 2-MC_6, 3-MC_6, 2-MC_{15}, 3-MC_{15}, 4-MC_{15}, and 5-MC_{15}), the energy profile is not symmetric. On Fig. 10b positions $2'$ and $4'$ representing the 2-MC_9 at the local energy maximum and at the global minimum, respectively, are not symmetric. In this case, the energy barrier can be decomposed into two smaller energy barriers. The nonsymmetric character of the molecule enhances its diffusion in the channel since the methyl group located close to the end of the chain makes the molecule relaxation easier during the diffusion. For those reasons, we confirm the result observed by Webb III (15, 16) using molecular dynamic calculations, that the diffusion depends on the methyl-branching position and that the more the branching is moved toward the center of the chain, the lower the diffusion barrier. However, our simulations provide a new insight on the origin of this phenomenon. It should be noticed that the effect of molecular symmetry on diffusion in restricted zeolite channels shown here, has never been reported previously. For MC_{15} paraffins the energy barrier increases till the methyl-branching position is 6. When the chain lengths on both sides of the methyl group are greater than five C–C bonds, the sterical hindrance has reached its maximum.

On Fig. 9, we report the relative values of the estimated diffusion coefficients for the monomethyl-branched paraffin versus the branching position. For calculating the relative diffusion coefficient, we ignore entropic effects and hence assume that all prefactors are equal at the given temperature. The trend shows clearly that the diffusion coefficient decreases strongly when the branching position moves from carbon number 2 to carbon number 4; then a plateau is reached for branching positions located between carbon number 5 to carbon number 8.

It is also shown in Table 6 that the energy barrier calculated for the 3-EC_5 of about +33.3 kJ/mol is higher than that of methyl-branched paraffins (even with longer chain except 6-MC_{15}). This high energy value is explained by the sterical hindrance of the ethyl group.

ZSM-23. For the monomethyl-branched C_7 isomers, the behavior is rather similar to the case of ZSM-22. The energy barrier for 2-MC_6 is lower than for 3-MC_6, which also confirms the result obtained by Webb (15, 16). However, as reported in Table 6, the energy barriers are higher in ZSM-23 than in ZSM-22 for linear and monomethyl-branched C_7-isomers.

EU-1. If we refer to (15, 16), the diffusion is also in favor of 2-MC_6 even if the diffusion selectivity is less pronounced in EU-1 than in ZSM-22. Actually this diffusion selectivity among monobranched products is essentially governed by the 10-MR channels present in ZSM-22, ZSM-23, or the 10-MR windows in EU-1.

2. *Dimethyl-Branched Products*

The molecular dynamic approach (15, 16) for studying monomethyl-branched isomers, has not been applied to dimethyl-branched isomers. Because of the lower diffusion coefficient of dimethyl-branched paraffins, it would require very high computer times to determine reliable values of diffusion coefficients. The diffusion-path approach is far less computer time consuming to investigate rapidly diffusion properties for dimethyl-branched paraffins. Although we are aware of its limitation (less accuracy in the evaluation of absolute energy barriers), the relative energy barriers for dimethyl-branched products can be calculated in a rather confident way as for monomethyl-branched isomers, provided that significant energy differences are found.

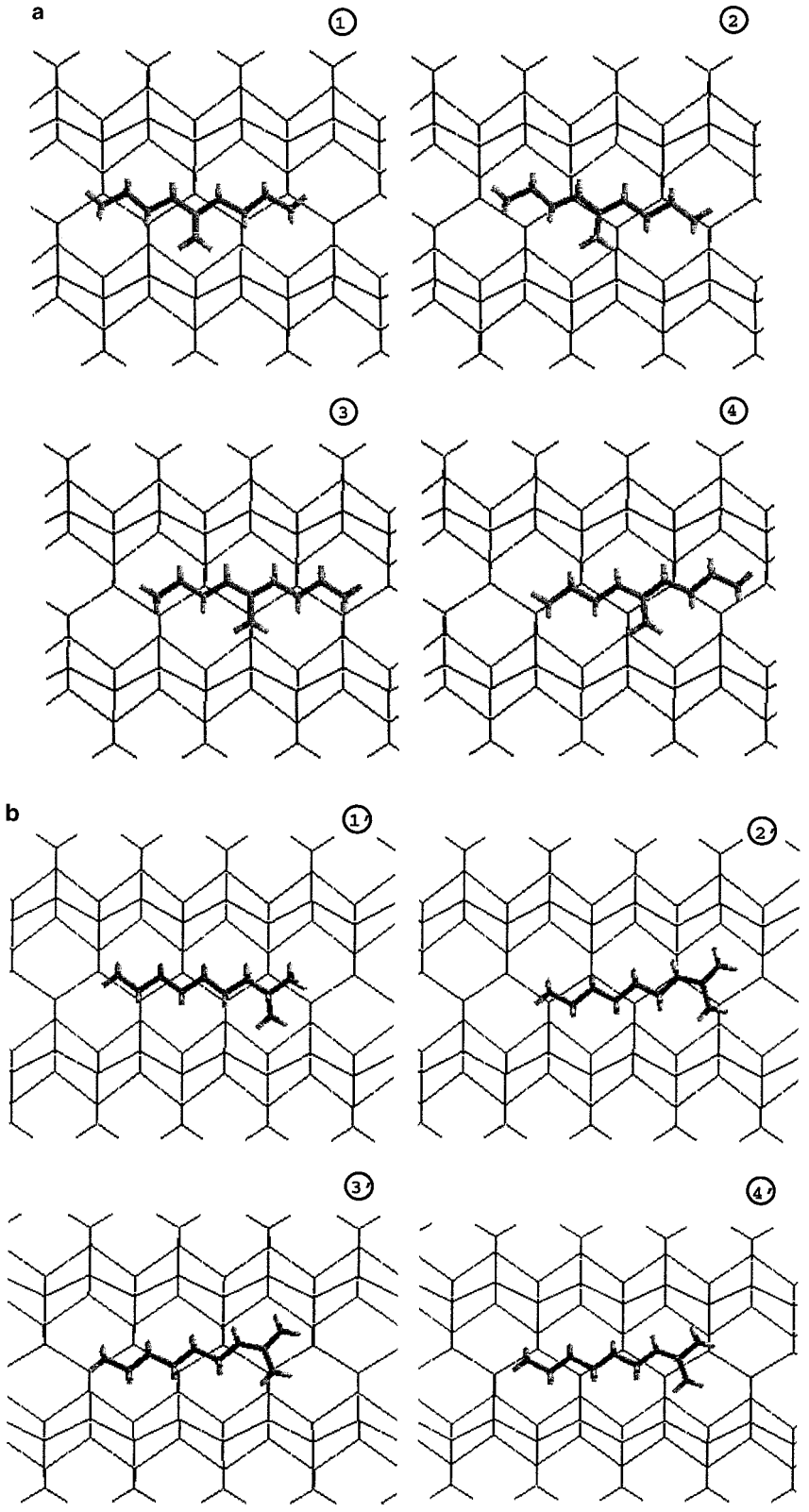

FIG. 8. Adsorption configurations of (a) 5-MC_9 and (b) 2-MC_9 along the diffusion path in the ZSM-22 (001) channel. The numbering stands for the configurations reported on the energy profiles of Fig. 7b.

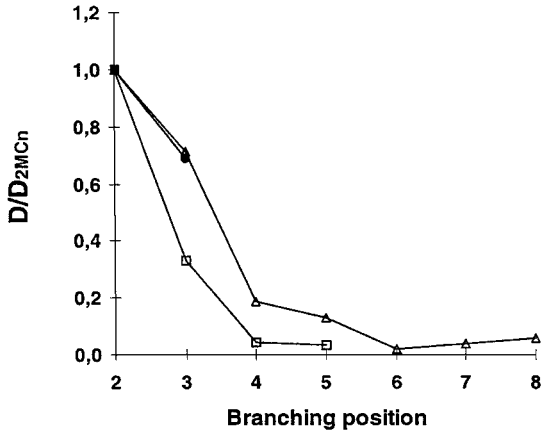

FIG. 9. Relative diffusion coefficient versus the branching position for MC_6 (black circles), MC_9 (squares), and MC_{15} (triangles). The reference for the diffusion coefficient is 2-MC_n and we assume that the diffusion prefactor is the same for all isomers.

ZSM-22. Figure 10a shows the energy profiles calculated for the dimethyl-branched C_5-isomers in ZSM-22. We observe first that the profile is far more perturbed than in the case of linear or monomethyl-branched products. This is explained by the strong roughness of the potential energy surface (PES) of dimethyl-branched paraffins in the channels of restricted zeolites. The energy barriers, reported in Table 7, reveal that the 2,2-dMC_5 and 3,3-dM_5 isomers are the slowest diffusing isomers. The branching of the two methyl groups on the same carbon atom is highly unfavorable for the compounds to diffuse through the channel. The molecule is blocked periodically by the repulsive interactions of the two methyl groups when crossing the barrier of the 10-MR channel. The energy barriers are about +92.2 and +83.3 kJ/mol for 2,2- and 3,3-dMC_5. For the 2,3- and 2,4-dMC_5, the diffusion is enhanced by the fact that the two methyl-groups behave as independent groups on the chain. So, it is easier for such molecules to find favorable configurations along the diffusion path than for 2,2- or 3,3-dMC_5. 2,4-dMC_5 exhibits the smallest diffusion barrier: +29.4 kJ/mol. 2,3-dMC_5 is an intermediate compound and its energy barrier is about +38.7 kJ/mol. It should be noticed also that these energy barriers are about 2 to 2.5 times higher than those of monomethyl-branched C_6.

It is also interesting to compare these results with the case of 3-EC_5 (Table 6). The diffusion barrier for this latter product is smaller than for 2,2- and 3,3-dMC_5. The ethyl group is flexible enough to allow atomic relaxations leading to smaller energy barrier in the 10-MR channel, whereas the

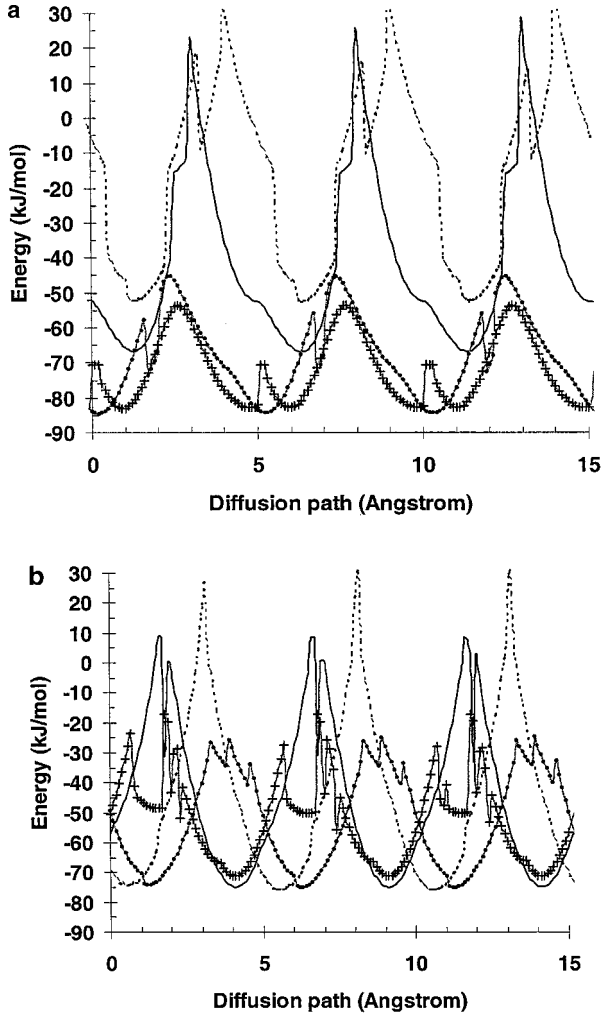

FIG. 10. Energy profiles along the diffusion path of 2,2-dMC_5 (—), 2,3-dMC_5 (•••), 2,4-dMC_5 (+++), and 3,3-dMC_5 (- - -) (a) inside the ZSM-22 (001) channel and (b) inside the ZSM-23 (100) channel.

TABLE 7

Energy Optima and Energy Barriers (kJ/mol) along the Diffusion Path of Dimethyl-Branched Isomers in ZSM-22, ZSM-23, and EU-1 Zeolites

	Energy minimum	Energy maximum	Energy barrier
ZSM-22			
2,2-dMC_5	−67.0	+25.2	+92.2
2,4-dMC_5	−83.0	−53.5	+29.4
3,3-dMC_5	−52.3	+31.1	+83.3
2,3-dMC_5	−84.3	−45.6	+38.7
ZSM-23			
2,2-dMC_5	−74.9	+9.8	+84.7
2,4-dMC_5	−71.3	−17.0	+54.4
3,3-dMC_5	−75.6	+30.7	+106.3
2,3-dMC_5	−75.1	−24.2	+50.9
EU-1			
2,2-dMC_5	−82.6	−16.2	+66.4
2,4-dMC_5	−83.8	−55.1	+28.7
3,3-dMC_5	−78.9	−8.2	+70.6
2,3-dMC_5	−87.9	−48.7	+39.2

Note. The energy values correspond to the energy profiles represented on Figs. 10a and 10b.

2,2-, 3,3-, and 2,3-dMC$_5$ are not. On the contrary, 2,4-dMC$_5$ diffuses faster than the 3-EC$_5$.

ZSM-23. The energy profiles obtained in ZSM-23 are shown on Fig. 10b. Although the main trends are governed by 10-MR pores, and are close to the ZSM-22 case, slight differences are observed. As in ZSM-22, the 2,3- and 2,4-dMC$_5$ compounds exhibit significantly smaller energy barriers (+50.9 and +54.4 kJ/mol, respectively) than 2,2- and 3,3-dMC$_5$ isomers (see Table 7). Nevertheless, we have to notice on the one hand that these barriers are higher in ZSM-23 than in ZSM-22 (as it has been observed for monomethyl-branched products). On the other hand, the diffusion barrier of the 2,4-dMC$_5$ is slightly higher than that of the 2,3-dMC$_5$.

EU-1. In this case, the determination of the diffusion path is more complicated, since the diffusion is anisotropic due to the large side pockets. The diffusion path approach makes it possible to investigate the diffusion barriers along the (100) direction only. We are aware of the important roles of the side pockets in trapping the linear or monomethyl-branched C$_7$ paraffins (15, 16) and diminishing significantly the diffusion coefficient of the products in this catalyst. The time of residence in the large side pockets is not investigated by our calculations and we assume that this contribution is rather similar for all the dimethyl products in 12-MR large side pockets. So even if we find smaller energy barriers in EU-1 than in ZSM-22 and ZSM-23, it would be false in this case to conclude that the products are diffusing faster in EU-1 than in ZSM-22 or ZSM-23. Recently Vlugt *et al.* (41) proposed a way of computing a free energy distribution path that could overcome this limitation. This approach will be considered in future works. Within the scope of this work, our goal is to evaluate the relative energy barriers of dimethyl-branched products along the (100) direction of the framework, the key parameter to understanding diffusion selectivity. Table 7 reports again a similar trend for the diffusion barriers of dimethyl-branched products. Since they have to diffuse through 10-MR windows bridging two large side pockets, it is not surprising that 2,2- and 3,3-dMC$_5$ diffuse slower than 2,4- and 2,3-dMC$_5$ products across the 10-MR bridges as observed in 10-MR channels of ZSM-22 or ZSM-23. The energy barriers are about +28.7 and +39.2 kJ/mol for 2,4- and 2,3-dMC$_5$, respectively.

3. 2,2,3-tMC$_4$ and Case of Y- and β-Zeolites

The energy barrier of 2,2,3-tMC$_4$ calculated in ZSM-22 is high: about +70.3 kJ/mol (see Fig. 11), but it is lower than for 2,2- or 3,3-dMC$_5$. Actually the adsorption energy, corresponding to the potential well on the energy profile, is weak (about −35.0 kJ/mol) so the 2,2,3-tMC$_4$ cannot be trapped, whereas 2,2- and 3,3-dMC$_5$ can be strongly adsorbed in some specific configurations. The absence of this strong potential well yields a lower energy barrier for the 2,2,3-tMC$_4$ product but this barrier is high enough to avoid diffusion of 2,2,3-tMC$_4$ out of the pores whenever it is formed. Furthermore, when we compare this result with the diffusion of 2,2,3-tMC$_4$ in β-zeolite along the (100) direction, it is shown clearly that no relevant diffusion restriction is observed in the open structure. As 2,2,3-tMC$_4$ is not limited by diffusion, there is no reason for monomethyl- and dimethyl-branched paraffins to be restricted by diffusion in open Y and β structures.

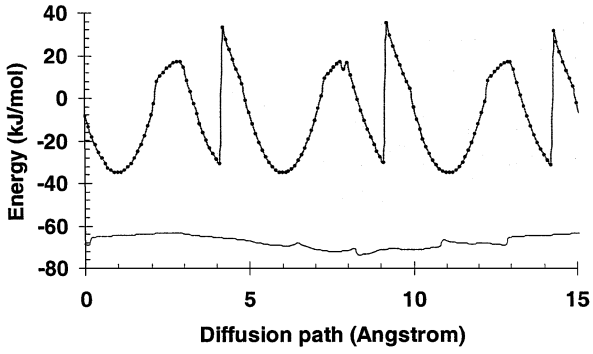

FIG. 11. Energy profiles along the diffusion path of 2,2,3-tMC$_4$ inside the ZSM-22 (001) channel (· · ·) and inside the β (001) channel (—).

DISCUSSION AND CONCLUSIONS

We consider first the formation of monomethyl-branched isomers. In 10-MR zeolites (ZSM-22, ZSM-23, or EU-1), the experimental selectivity ratio (2-MC$_6$/3-MC$_6$) is in favor of the 2-MC$_6$ as shown on Fig. 12a, whereas in 12-MR zeolites no selectivity is observed. Isomerization reactions (1) and (2) on Fig. 6a show that the shape transition state selectivity cannot by itself explain the experimental results. Even if reaction (2) is unfavored, reaction (1) leads to the formation of both 2- and 3-MC$_6$. So the diffusion limitation of the 3-MC$_6$ governs mainly the selectivity observed in ZSM-22, ZSM-23, or EU-1. In Y- and β-zeolites, there is neither shape transition state selectivity nor diffusion limitation, so the (2MC$_6$/3MC$_6$) ratio is significantly smaller (close to 1). On Fig. 12a, we notice that the experimental selectivity in 2-MC$_6$ is less pronounced in EU-1 than in other restricted structures. In the large side pockets, CP(1) and CP(2) stabilities are similar (see Table 5), so reaction (1) may occur easier than in ZSM-22. Therefore a greater quantity of 3-MC$_6$ is detected and can diffuse out of the pore decreasing the selectivity in 2-MC$_6$ isomer. Furthermore, according to (15, 16) the diffusion selectivity of 2-MC$_6$ is less pronounced in EU-1 than in ZSM-22 and ZSM-23.

For dimethyl-branched isomers, the experimental selectivities in restricted zeolites such as ZSM-22 and ZSM-23 reveal that 2,3- and 2,4-dMC$_5$ are formed preferentially as shown on Fig. 12b. The calculated diffusion barriers have shown than 2,3- and 2,4-dMC$_5$ are the faster diffusing dimethyl-branched isomers in 10-MR zeolites with

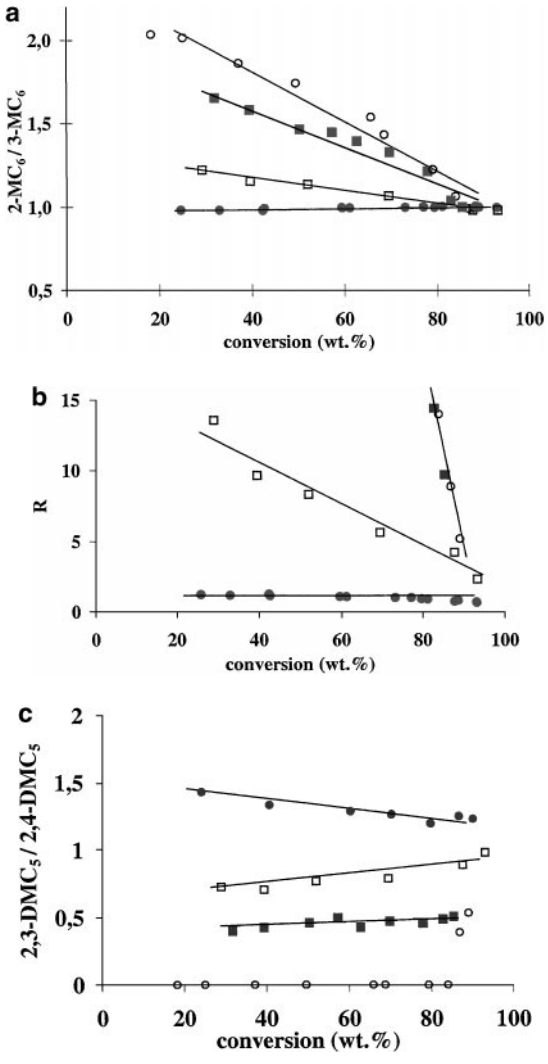

FIG. 12. (a) (2-MC_6/3-MC_6) ratio versus *n*-heptane conversion (●) Pt/H-Y or Pt/H-β, (○) Pt/ZSM-22, (■) Pt/ZSM-23, (□) Pt/EU-1; (b) (2,3-dMC_5 + 2,4-dMC_5)/(2,2-dMC_5 + 3,3-dMC_5) ratio (R) versus *n*-heptane conversion; (c) (2,3-dMC_5/2,4-dMC_5) ratio versus *n*-heptane conversion.

reasonable energy barriers. 2,2- and 3,3-dMC_5 are definitively excluded by diffusion limitation (the barriers are greater than 80 kJ/mol in ZSM-22 and ZSM-23). It should be emphasized that this result is in agreement with a recent *in situ* IR spectroscopy study of Pieterse *et al.* (42) showing that 2,2-dMC_5 are unable to fully enter the pores of ZSM-22. Furthermore, in the present study, we show that 2,2- and 3,3-dMC_5 are first excluded by TS selectivity. We observe slight differences between ZSM-22 and ZSM-23. In ZSM-22, there is hardly any 2,3-dMC_5 produced, as is shown on Fig. 12c, except at very high conversion. The simulation shows that the diffusion barrier is greater for 2,3-dMC_5 than for 2,4-dMC_5 in ZSM-22. The diffusion barrier of the 2-EC_5 is even lower than that of 2,3-dMC_5. So 2,3-dMC_5 can diffuse out of the ZSM-22 pores only with great difficulty, like 2-EC_5 does. 2,3-dMC_5 is therefore mainly transformed by methyl shift in 2,4-dMC_5 or cracked through reaction (7), yielding *n*-C_4. Indeed we notice on Table 3 that the amount of nC_4 is slightly higher in ZSM-22 than in ZSM-23 or EU-1. In ZSM-23, the 2,3-dMC_5 diffuses faster than 2,4-dMC_5. So a nonnegligible amount of 2,3-dMC_5 is observed experimentally and a smaller amount of nC_4 is detected.

Finally we have to focus on the EU-1 case exhibiting the highest amount of cracked products among the restricted structures. Although we are aware that this could also depend on the acidic properties of the different catalysts, the CP stability and diffusion limitation give interesting insights. We have plotted on Figs. 13a and 13b energy profiles for the reaction paths (3), (4), and (5) involving 2-MC_6 and 3-MC_6 as reactants and CP(3), CP(4), and CP(5) as intermediates for ZSM-22 and EU-1, respectively. The energy diagrams show that the environment is favorable to CP(4) in ZSM-22, whereas in EU-1 no shape transition state selectivity because environment effects take place inside the large side pockets, as if they were small Y- or β-catalyst units. In ZSM-22, the 2,3- and 2,4-dMC_5 products are the main products through the stable CP(4), and they account for only a small amount of cracking since they are also the faster diffusing compounds. Whereas in ZSM-22, the 2,2- and 3,3-dMC_5 are excluded by shape TS selectivity, in EU-1, all dimethyl-branched isomers are formed inside the 12-MR pockets without shape TS selectivity. This explains first the higher amount of 2,3-isomers than in ZSM-22 or ZSM-23. Then as 2,2- and 3,3-dMC_5 cannot diffuse out of the 10-MR window, 2,2-dMC_5 will crack inside the large

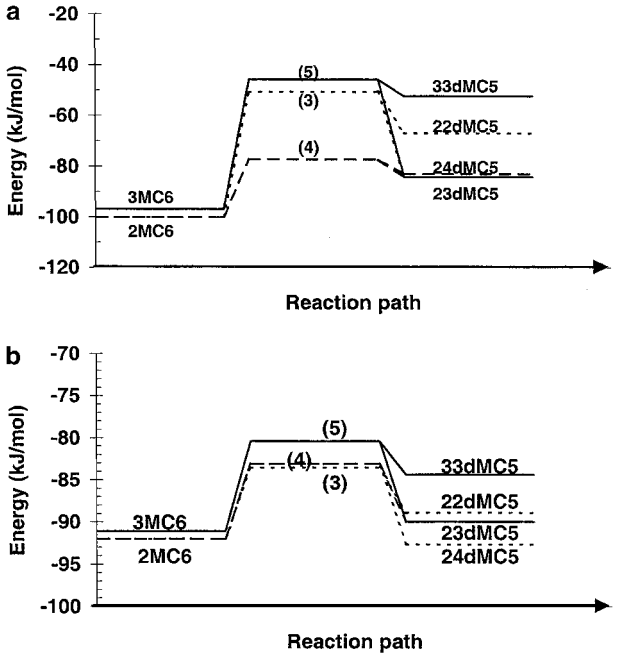

FIG. 13. Energy diagrams for the reaction path of the MC_6 isomerizations into dMC_5 through cyclopropane (CP) intermediates (see also Fig. 6 and explanation in text). (a) in ZSM-22 and (b) in EU-1.

side pockets and form an additional amount of C_3 and iC_4 while 3,3-dMC_5 is transformed via methyl shift.

Finally, on open structures, no diffusion restriction or shape transition state selectivity (in the sense of long range interactions) takes place. None of the dimethyl-isomers is excluded by shape selectivity, and the hydroconversion selectivity is mainly controlled by the relative stabilities of the different transition states involved in isomerization, methyl-shift, and cracking reactions.

Considering the results from molecular diffusion path simulations and CP stabilities, we have proposed an interpretation of the experimental selectivities. We have established for the first time the diffusion properties of dimethyl-branched paraffins inside such restricted structures. In particular for understanding C_7-hydroconversion selectivities in ZSM-22, ZSM-23, and EU-1, it has not been required to invoke the "pore mouth" concept. The coupled effect between shape transition state selectivity and diffusion limitations on restricted structures seems to be the best way of explaining the experimental selectivities observed in the various di-branched isomers and in the cracked products.

As we have emphasized that the interaction of the PCP ring with the acidic site is crucial for understanding C_7-hydroconversion selectivities, particularly on open structures, it would be required to calculate true transition states structure and energetics at the density functional theory (DFT) level. Recent studies in this area are very promising (43, 44) and should bring a lot of new insights in the future.

ACKNOWLEDGMENTS

We thank our colleagues: Ch. Marcilly, Ch. Travers, E. Benazzi, S. Lacombe, and L. Rouleau from Institut Français du Pétrole (IFP) for very interesting scientific discussions and fruitful collaboration and the Laboratoire des Matériaux Minéraux (Mulhouse) for having performed the ZSM-22 synthesis.

REFERENCES

1. Belloum, M., Travers, Ch., and Bournonville, J. P., *Rev. Inst. Fr. Pét.* **46**(1), 89 (1991).
2. Weisz, P. B., *Adv. Catal.* **13**, 137 (1962).
3. Coonradt, H. L., and Garwood, W. E., *Ind. Eng. Chem. Proc. Res. Dev.* **3**, 38 (1964).
4. Weitkamp, J., and Schultz, H., *J. Catal.* **29**, 361 (1973).
5. Chevalier, F., Guisnet, M., and Maurel, T., *C. R. Acad. Sci. Paris* **282**, 3 (1976).
6. Weisz, P. B., and Swegler, E. W., *Science* **126**, 31 (1957).
7. Horiuti, J., and Polanyi, M., *Trans. Faraday Soc.* **30**, 1164 (1934).
8. Weitkamp, J., *J. Ind. Eng. Chem. Prod. Res. Dev.* **21**, 550 (1982).
9. Gianetto, G. E., Perot, G. R., and Guisnet, M., *Ind. Eng. Chem. Prod. Res. Dev.* **25**, 481 (1986).
10. Brouwer, D. M., and Oelderick, J. M., *Recl. Trav. Chim. Pays-Bas* **87**, 721 (1968).
11. Chevalier, F., Guisnet, M., and Maurel, R., "Proceedings, 6th International Congress on Catalysis, London, 1976" (G. C. Bond, P. B. Wells, and F. C. Thompkins, Eds.), The Chemical Society, London, 1977.
12. Pichler, H., Schulz, H., Reitemeyer, H. O., Weitkamp, J., and Erdöl, J., *Kohle-Erdgas-Petrochem.* **25**, 494 (1972).
13. Csicsery, S. M., *Zeolites* **4**, 202 (1984).
14. Derouane, E. G., *Stud. Surf. Sci. Catal.* **5**, Eds. B. Imelik *et al.*, Elsevier, Amsterdam (1980) p5.
15. Webb, E. B., III, and Grest, G. S., *Catal. Lett.* **56**, 95 (1999).
16. Webb, E. B., III, Grest, G. S., and Mondello, M., *J. Phys. Chem. B* **103**, 4949 (1999).
17. Ernst, S., Weitkamp, J., Martens, J. A., and Jacobs, P. A., *Appl. Catal.* **48**, 137 (1989).
18. Meriaudeau, P., Tuan, Vu. A., Sapaly, G., Nghiem, Vu. T., and Naccache, C., *Catal. Today* **49**, 285 (1999).
19. Maesen, Th. L. M., Schenk, M., Vlugt, T. J. H., de Jonge, J. P., and Smit, B., *J. Catal.* **188**, 403 (1999).
20. Martens, J. A., Parton, R., Uytterhoeven, L., and Jacobs, P. A., *Appl. Catal.* **76**, 95 (1991).
21. Souverjins, W., Martens, J. A., Uytterhoeven, L., Froment, G. F., and Jacobs, P. A., *Prog. Zeolite Microporous Mater.* **105**, 1285 (1997).
22. Denayer, J. F., Baron, G. V., Vanbutsele, G., Jacobs, P. A., and Martens, J. A., *Chem. Ing. Sci.* **54**, 3553 (1999).
23. Claude, M. C., and Martens, J. A., *J. Catal.* **190**, 39 (2000).
24. Patrigeon, A., Benazzi, E., Travers, Ch., and Bernhard, J. Y., "4th European Congress on Catalysis, EUROPACAT-IV, Rimini, Italy, September 5–10, 1999." Book of Abstracts.
25. Newsam *et al. Nature* **349**, 508 (1991).
26. Newsam, J. M., Treacy, M. M. J., Koetsier, W. T., and deGruyter, C. B., *Proc. R. Soc. London A* **420**, 375 (1988).
27. Kokotailo, G. T., Schlenker, J. L., Dwyer, F. G., and Valyocsik, E. W., *Zeolites* **5**, 349 (1985).
28. Rohrman, A. C., LaPierre, R. B., Schlenker, J. L., Wood, J. D., Valyocsik, E. W., Rubin, M. K., Higgins, J. B., and Rohrbaugh, W. J., *Zeolites* **5**, 352 (1985).
29. Briscoe, N. A., Johnson, D. W., Shannon, M. D., Kokotailo, G. T., and McCusker, L. B., *Zeolites* **8**, 74 (1988).
30. Souverjins, W., Rombouts, L., Martens, J. A., and Jacobs, P. A., *Microporous Mater.* **4**, 123 (1995).
31. Casci, J. L., Lowe, B. M., and Whittam, T. V., Patent EP B1 042 226 (1984).
32. Zones, S. I., Ziemer, J. N., Santilli, D. S., Innes, R. A., and Holtermann, D. L., U.S. patent 5,300,210 (1993).
33. Lowe, B. M., and Araya, A., Patent EP-A2 077 624 (1983).
34. Compass, Sorption, and Diffusion_Path are ditributed with MSI's software package *InsightII* and *Cerius*^{2} (*InsightII* and *Cerius*^{2} User Guides).
35. Horsley, J. A., Fellmann, J. D., Derouane, E. G., and Freeman, C. M., *J. Catal.* **147**, 231 (1994).
36. Sun, J., *J. Phys. Chem. B* **102**, 7338 (1998).
37. Maple, J. R., Dinur, U., and Hagler, A. T., *Proc. Natl. Acad. Sci. USA* **85**, 5350 (1988).
38. Alen, M. P., and Tildesley, D. J., Computer Simulation of Liquids; Oxford University Press: Oxford (1989).
39. Denayer, J. F., Souverijns, W., Jacobs, P. A., Martens, J. A., and Baron, G. V., *J. Phys. Chem. B* **102**, 4588 (1998).
40. Vlugt, T. J. H., Krishna, R., and Smit, B., *J. Phys. Chem. B* **103**, 1102 (1999).
41. Vlugt, T., Smit, B., and Krishna, R., "Proceedings, 12th International Zeolite Conference" (M. M. J. Treacy, *et al.*, Eds.), Vol. 1, p. 325. Materials Research Society, Warrendale, PA, 1998.
42. Pieterse, J. A. Z., Veefkind-Reyes, S., Seshan, K., and Lercher, J. A., *J. Phys. Chem. B* **104**, 5715 (2000).
43. Van Santen, R. A., *Catal. Today* **38**, 377 (1997).
44. Jeanvoine, Y., Angyan, J., Kresse, G., and Hafner, J., *J. Phys. Chem. B* **102**, 5573 (1998); Demuth, T., Hafner, J., Benco, L., and Toulhoat, H., *J. Phys. Chem. B* **104**, 4593 (2000).